Special Issue of the 7th International Advances in Applied Physics and Materials Science (APMAS 2017)

Fe_2O_3/Y_2O_3 Catalyst Supported on Alumina and Halloysite

M. Karaismailoglu*, H.E. Figen and S.Z. Baykara
Chemical Engineering Dept., Yildiz Technical University, Topkapi, Istanbul 34210, Turkey

Fe_2O_3/Y_2O_3 metal oxide catalysts on different supports have been developed for the removal of catalytic topping atmosphere residue. All catalysts have been prepared by the sol-gel citrate method where citric acid was used as a complexing agent. Alumina and halloysite were used as catalyst supports due to their high surface areas. The prepared samples were structurally characterized by X-ray diffraction, Brunauer-Emmett-Teller measurements and by scanning electron microscopy techniques. X-ray diffraction results for the catalysts were as follows: $Fe_2O_3/Y_2O_3/Al_2O_3(Al_3Fe_2O_{12}Y_3)$ and Fe_2O_3/Y_2O_3/Halloysite ($Al_2Fe_3O_{12}Y_3$, O_2Si, $Al_{4.52}O_{9.74}Si_{1.48}$). Brunauer-Emmett-Teller surfaces were in the range of 23–31 m^2/g for $Fe_2O_3/Y_2O_3/Al_2O_3$ and 1–9 m^2/g for Fe_2O_3/Y_2O_3/Halloysite.

DOI: 10.12693/APhysPolA.134.57
PACS/topics: Fe_2O_3/Y_2O_3, alumina, halloysite, topping atmosphere residue, TAR

1. Introduction

With the growth in world population the energy demand increases. Fossil fuel resources are depleting and their combustion leads to high amount of carbon dioxide gas (CO_2), resulting in global warming. For reducing the dependence on fossil fuels and the CO_2 emission, the interest in renewable energy resources like solar, wind, geothermal, hydrogen and biomass is growing. Biomass attracts extra attention because plants capture the CO_2 gas through the photosynthesis.

There are bio- and thermochemical processes of conversion of the biomass into the desired products. Pyrolysis and gasification of biomass are two of the most known thermochemical methods [1]. In the presence of gasifying agents such as oxygen or steam, biomass can be converted into value added industrial products like hydrogen (H_2) and methane (CH_4) [2]. Carbon monoxide (CO), carbon dioxide (CO_2), nitrogen (N_2), ammonia (NH_3), hydrogen sulfide and topping atmosphere residue (TAR) compounds are some of other products [2].

TAR compounds, which contain long chains or aromatic hydrocarbons, can easily condense. High concentration of TAR compounds can plug the equipment and the active sites of catalysts [3]. Hence, optimization of reaction conditions and development of metal oxide catalysts are important research areas for removal of TAR compounds.

Nickel (Ni) based catalysts are mostly used for TAR conversion because of their high activity. However, carbon formation on the catalyst surface causes deactivation [4, 5]. Hence, other metal catalysts were developed and their activity tests were performed. Catalysts which contain noble metals like rhodium (Rh), ruthenium (Ru) and platinum (Pt) were also investigated and it was found that these types of metal catalysts had high catalytic activity and selectivity. They also have high resistivity to hydrogen sulfide [6, 7]. However, noble metal based catalysts are more expensive compared to Ni-based catalysts. Hence, less pricey cobalt (Co), iron (Fe), zinc (Zn) and copper (Cu) based catalysts were synthesized and tested. It was found that the addition of these metals had increased the catalytic activity and reduced carbon formation [3, 8, 9].

Support materials have been widely used in heterogeneous catalysis because of their high surface area [1]. The active phases can easily disperse on the support and increase catalytic activity. Alumina (Al_2O_3) and halloysite ($Si_2Al_2O_5(OH)_4{\cdot}2H_2O$) are two examples of materials which are widely used as catalyst support [10].

Halloysite is a kaolinite type material which consists of layered [SiO_4] and [AlO_4] polyhedrons. This mineral has nanotube structure. The performance of metal loaded halloysite was investigated and it was concluded that palladium (Pd), cobalt oxide (Co_3O_4) or zinc sulfide (ZnS) loaded on halloysite show excellent catalytic activity [11].

In the present work, we have aimed to develop metal oxide catalysts with high resistivity to the corrosive H_2S, to convert the TAR compounds into H_2 and CH_4 gases. Yttrium (Y) and iron (Fe) containing catalysts were synthesized by sol-gel citrate method. Alumina and halloysite were used as supports. X-ray diffraction (XRD), Brunauer Emmett Teller (BET) and scanning electron microscopy with energy dispersive spectroscopy (SEM-EDS) analyses were performed for structural characterization of each of the synthesized catalysts.

2. Materials and methods

2.1. Catalyst preparation

Yttrium and iron oxide (Y_2O_3/Fe_2O_3) type catalysts were synthesized by the sol-gel method and citric acid was used as a sol-gel agent. Appropriate amounts of yttrium nitrate hexahydrate ($Y(NO_3)_3{\cdot}6H_2O$, ABCR GmbH) and iron nitrate nonahydrate ($Fe(NO_3)_3{\cdot}9H_2O$, Alfa Aesar) were used to prepare 1 M precursor solutions. Citric acid was added to the precursor solution

*corresponding author; e-mail: meltemkoglu@hotmail.com

and it was mixed overnight. After 1 M ammonium carbonate $(NH_4)_2CO_3$ solution was added for adjusting the pH to 6, the solution was evaporated at 80 °C and the precursor solution became a viscous gel.

The catalyst was dried at 210 °C in an oven and was calcined at 1000 °C for 5 h. For loading of the catalysts on different supports ($Y_2O_3/Fe_2O_3/Al_2O_3$ and Y_2O_3/Fe_2O_3/halloysite), appropriate amounts of support materials (aluminium oxide anhydrous (Merck) and halloysite (ESAN)) were added to the precursor solution.

2.2. Catalyst characterization

XRD analyses of the synthesized catalysts were performed for determination of their crystal structure and were carried out at ambient temperature using a Philips Panalytical X'Pert-Pro diffractometer in an angle range of 10°–70° with Cu K_α radiation at operating parameters of 40 mA and 45 kV with a step size of 0.02 and scan speed of 0.04°/s.

BET surface areas of the catalysts were determined using Micromeritcs Gemini VII BET instrument. After the samples were degassed at 300 °C, their specific surface areas were determined under N_2 adsorption. The microstructure and morphology of the samples were examined by using scanning electron microscopy ZEISS EVO LS 10 (SEM) coupled with energy dispersive X-ray spectroscopy (EDS) for the analysis of metal contents.

3. Results and discussion

3.1. X-ray diffraction

XRD patterns of the alumina and halloysite supported catalysts are given in Fig. 1 and crystalline phase parameters are listed in Table I. It is observed that the influence of support is manifested in the presence of different crystal phases and garnet structures. The sample of series A-1 with $Fe(NO_3)_3/Y(NO_3)_3$ molar ratio 1:1 contains a single phase garnet structure of $Al_4FeO_{12}Y_3$.

Catalyst of series A-2, which was prepared with the $Fe(NO_3)_3/Y(NO_3)_3$ molar ratio 1:2, also shows a garnet structure but with a different chemical formula of $Al_2Fe_3O_{12}Y_3$. Catalyst of series A-2 and A-4 with higher quantity of yttrium nitrate have similar garnet structures ($Al_2Fe_3O_{12}Y_3$ and $Al_3Fe_2O_{12}Y_3$, respectively). They also contain yttria and magnetite phases.

Samples prepared with the larger quantity of iron nitrate (series of A-3 and A-5) contain the same crystal phases with different intensities. Catalyst of series A-5 shows a higher intensity for the Fe_2O_3 peaks at $2\theta = 24.202°$, 40.954°, 54.203°, 64.149° and 72.150°.

Halloysite has a more complex structure, which leads to the formation of multi phases in catalyst samples. Calcination of halloysite at high temperatures causes dehydration and phase transformation [3, 12]. Therefore, catalysts with halloysite support contain such crystal phases as cristobalite (O_2Si) and mullite ($Al_{452}O_{9.74}Si_{1.48}$).

Catalyst series of H-1 has the highest quantity of iron and yttrium nitrate and contains two different garnet

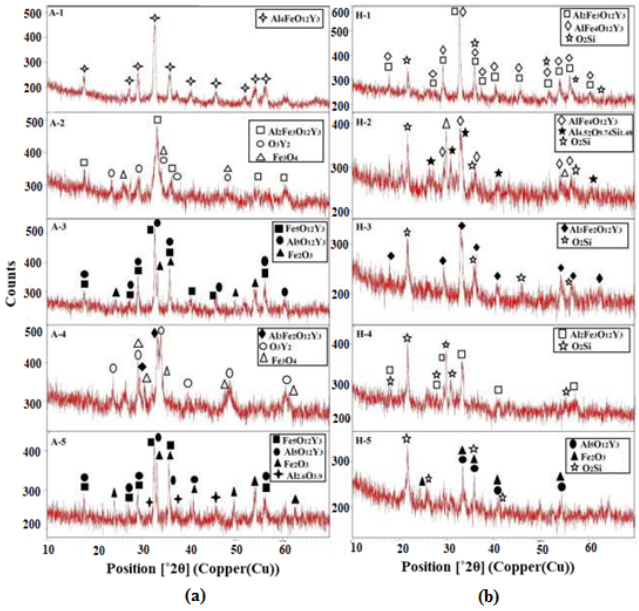

Fig. 1. XRD patterns of alumina (a) and halloysite (b) supported catalysts.

structures such as $AlFe_4O_{12}Y_3$ and $Al_2Fe_3O_{12}Y_3$. Reduction of the amount of iron nitrate leads to the formation of a single garnet structure in catalyst series of H-2 and H-4. Catalyst series of H-5 has the lowest quantity of yttrium nitrate and contains a different type of garnet structure (such as $Al_5O_{12}Y_3$) compared to the other halloysite based catalysts. Besides, except for the catalyst series of H-5 non of the halloysite supported samples indicates any metal oxide type crystal structure. With the increase in $Fe(NO_3)_3/Y(NO_3)_3$ molar ratio the metal oxide crystal phases can be present.

3.2. BET surface area

Results of specific surface area (BET) measurements of the catalysts are given in Table II. Alumina and halloysite were used as support materials because of their high specific surface areas. It is observed that the exposure of the supports to high temperature reduces their specific surface areas. The surface area of halloysite decreases from 134.79 to 8.2717 m^2/g after the calcination. High temperatures change the morphological structure of halloysite, which leads to a decrease in porosity. Catalysts of series A-1 and H-1 with the same $Fe(NO_3)_3/Y(NO_3)_3$ molar ratio have surface areas of 23.8861 and 8.2105 m^2/g, respectively. It was found that with the increase in molar content of $Y(NO_3)_3$ the BET surface area decreases. Catalysts of series H-2 with the molar ratio of $Fe(NO_3)_3/Y(NO_3)_3$ 1:2 has 3.5752 m^2/g and series H-4 with the $Fe(NO_3)_3/Y(NO_3)_3$ molar ratio 1:3 has 1.1719 m^2/g surface areas.

However, this correlation for the alumina containing catalysts is completely different. A higher molar content of $Y(NO_3)_3$ leads to the increase of specific surface areas

TABLE I

Crystalline phase content of the synthesized catalysts. Sample codes starting with A and H indicate alumina and halloysite support, respectively.

Sample	Molar ratio	Crystal phases	Reference code	Crystal system
A-1	1:1	$Al_4FeO_{12}Y_3$	98-009-3633	Cubic
A-2	1:2	$Al_2Fe_3O_{12}Y_3$	98-009-3628	Cubic
		Y_2O_3	98-015-3500	Cubic
		Fe_3O_4	98-008-7697	Orthorhombic
A-3	2:1	Fe_2O_3	98-008-2135	Hexagonal
		$Fe_5O_{12}Y_3$	98-017-3997	Cubic
		$Al_5O_{12}Y_3$	98-017-0158	Cubic
A-4	1:3	Y_2O_3	98-015-3500	Cubic
		Fe_3O_4	98-003-5001	Orthorhombic
		$Al_3Fe_2O_{12}Y_3$	98-009-3631	Cubic
A-5	3:1	Fe_2O_3	98-020-1097	Hexagonal
		$Fe_5O_{12}Y_3$	98-017-3997	Cubic
		$Al_5O_{12}Y_3$	98-017-0158	Cubic
		$Al_{2.666}O_{3.999}$	98-009-9836	Tetragonal
H-1	1:1	$AlFe_4O_{12}Y_3$	98-009-3626	Cubic
		$Al_2Fe_3O_{12}Y_3$	98-009-3628	Cubic
		O_2Si	98-007-7454	Tetragonal
H-2	1:2	$AlFe_4O_{12}Y_3$	98-009-3626	Cubic
		$Al_{4.52}O_{9.74}Si_{1.48}$	98-006-6451	Orthorhombic
		O_2Si	98-004-4269	Cubic
H-3	2:1	$Al_3Fe_2O_{12}Y_3$	98-009-3631	Cubic
		O_2Si	98-007-7463	Cubic
H-4	1:3	$Al_2Fe_3O_{12}Y_3$	98-009-3628	Cubic
		O_2Si	98-004-4269	Cubic
H-5	3:1	$Al_5O_{12}Y_3$	98-004-1144	Cubic
		Fe_2O_3	98-008-2136	Hexagonal
		O_2Si	98-008-9292	Hexagonal

TABLE II

Specific surface area of the catalysts.

Sample	Molar ratio	Support	BET [m^2/g]
A-1	1:1	Alumina	23.8861
A-2	1:2	Alumina	24.3357
A-3	2:1	Alumina	20.3056
A-4	1:3	Alumina	30.8322
A-5	3:1	Alumina	24.0542
H-1	1:1	Halloysite	8.2105
H-2	1:2	Halloysite	3.5752
H-3	2:1	Halloysite	6.6364
H-4	1:3	Halloysite	1.1719
H-5	3:1	Halloysite	4.0473
		Alumina	126.6675
A-0		Alumina*	43.1587
		Halloysite	134.79
H-0		Halloysite*	8.2717

*Calcined at 1000 °C

of the catalysts of series A-2 and A-4. It is believed that the dispersion of yttrium in halloysite is much stronger than in alumina. Hence, halloysite supported catalysts with same molar ratio of $Fe(NO_3)_3/Y(NO_3)_3$ have lower surface areas compared to alumina supported samples.

3.3. Scanning electron microscopy

The microstructure of prepared catalysts was determined using SEM. The samples were fixed to the sample holder with carbon adhesive tape. Figure 2 shows SEM micrographs at 40 000× magnification for samples A-0, A-1, A-2, A-3 A-4 and A-5. Catalysts series of A-1 to A-5, which contain alumina support, have similar SEM images. Particles of all alumina supported catalysts display agglomeration.

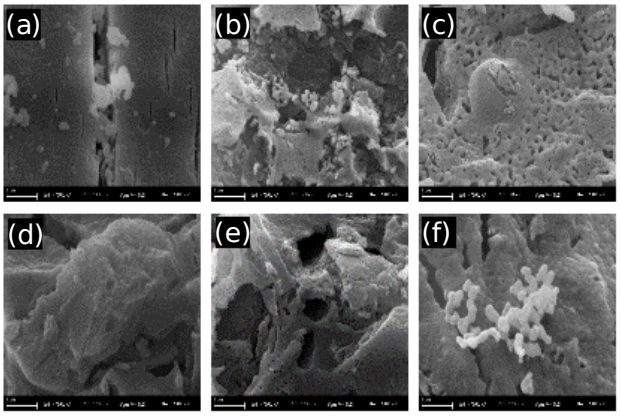

Fig. 2. SEM micrographs (a)-(f) of the catalyst series of A-0, A-1, A-2, A-3, A-4 and A-5, rspectively.

Figure 3 shows SEM micrographs at 10 000× magnification for H-0, H-2 and H-3 samples and at 20 000× magnification for H-1, H-4 and H-5 samples. Agglomeration is observed in all halloysite supported samples.

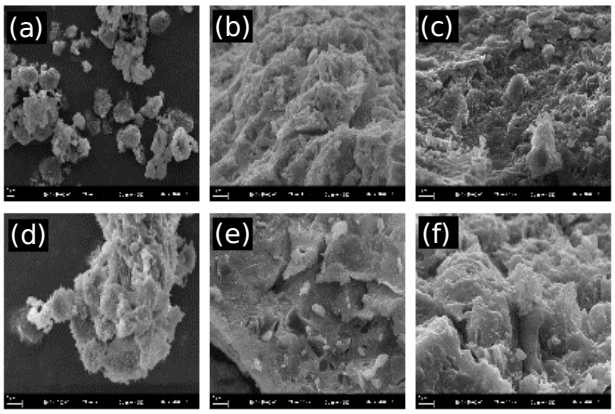

Fig. 3. SEM micrographs (a)-(f) of the catalyst series of H-0, H-1, H-2, H-3, H-4 and H-5, respectively.

TABLE III
Quantitative results of weight ratio of selected elements according to EDS analysis.

Sample	Molar ratio	Support	Element lines	Content [wt.%]	Error [wt.%]
A-1	1:1	Alumina	Fe K	19.7	4.8
			Y L	19.8	3.7
A-2	1:2	Alumina	Fe K	10.3	7.4
			Y L	24.5	4.2
A-3	2:1	Alumina	Fe K	43.6	3.4
			Y L	23.5	3.4
A-4	1:3	Alumina	Fe K	29.7	5.2
			Y L	51.3	3.3
A-5	3:1	Alumina	Fe K	27.8	3.5
			Y L	13.0	3.7
H-1	1:1	Halloysite	Fe K	12.3	7.2
			Y L	12.7	5.3
H-2	1:2	Halloysite	Fe K	10.2	6.1
			Y L	22.8	3.7
H-3	2:1	Halloysite	Fe K	18.2	4.6
			Y L	9.1	5.3
H-4	1:3	Halloysite	Y L	6.5	10.6
			Y L	15.6	4.8
H-5	3:1	Halloysite	Fe K	23.4	4.6
			Y L	8.4	6.7

4. Conclusions

According to the XRD results, multiphase structural catalysts were obtained. The addition of support materials has led to the presence of various cubic garnet-type structures. Alumina supported catalyst with the $Fe(NO_3)_3/Y(NO_3)_3$ molar ratio 1:1 displays a single phase crystal structure. With the increase in $Fe(NO_3)_3/Y(NO_3)_3$ molar ratio, multiphase structural catalysts were obtained and application of halloysite as the support has led to the formation of a single garnet structure.

The BET results have confirmed that the addition of support increases the specific surface areas of metal oxide catalysts. Alumina supported catalysts have higher specific surface areas compared to halloysite supported catalysts. The SEM micrographs of alumina and halloysite supported catalysts have displayed agglomerates.

Acknowledgments

This research is supported by the Scientific and Technological Research Council of Turkey (TUBITAK-MAG, Project No: 213M368) and Research Fund of the Yildiz Technical University (YTU, Project No: 2016-07-01-DOP01).

References

[1] G. Guan, *Renewable Sustainable Energy Rev.* **58**, 450 (2016).

[2] J.A. Ruiz, M.C. Juarez, M.P. Morales, P. Munoz, M.A. Mendivil, *Renewable Sustainable Energy Rev.* **18**, 174 (2013).

[3] T. Furusawa, A. Tsutsumi, *Appl. Catal. A* **278**, 207 (2005).

[4] D. Swierczynski, S. Libs, C. Courson, A. Kiennemann, *Appl. Catal. B* **74**, 211 (2007).

[5] T. Miyazawa, T. Kimura, J. Nishikawa, S. Kado, K. Kunimori, K. Tomishige, *Catal. Today* **115**, 254 (2006).

[6] T. Furusawa, K. Saito, Y. Kori, Y. Miura, M. Sato, N. Suzuki, *Fuel* **103**, 111 (2013).

[7] K. Polychronoppulou, J.L.G. Fierro, A.M. Efstathiou, *J. Catal.* **228**, 417 (2004).

[8] D. Li, C. Ishikawa, M. Koike, L. Wang, Y. Nakagawa, K. Tomishige, *Int. J. Hydrogen Energy* **38**, 3572 (2013).

[9] K. Polychronopoulou, A. Bakandritsos, V. Tzitzios, J.L.G. Fierro, A.M. Efstathiou, *J. Catal.* **241**, 132 (2006).

[10] A.M. Carillo, J.G. Carriazo, *Appl. Catal. B* **164**, 443 (2015).

[11] J. Ouyang, Z. Zhou, Y. Zhang, H. Yang, *Appl. Clay Sci.* **101**, 16 (2014).

[12] P. Yuan, D. Tan, F.A. Bergaya, W. Yan, M. Fan, D. Liu, H. Ha, *Clays Clay Miner.* **60**, 561 (2012).